TIME-DOMAIN FORMULATION OF A PERFECTLY MATCHED LAYER FOR THE SECOND-ORDER ELASTIC WAVE EQUATION WITH VTI MEDIA

JAEJOON LEE[1] and CHANGSOO SHIN[2]

[1] *Computational Science and Technology Program, Seoul National University, Seoul, South Korea. joons86@snu.ac.kr*
[2] *Department of Energy System Engineering, Seoul National University, Seoul, South Korea. css@model.snu.ac.kr*

(Received November 7, 2014; revised version accepted April 12, 2015)

ABSTRACT

Lee, J. and Shin, C.S., 2015. Time-domain formulation of a perfectly matched layer for the second-order elastic wave equation with VTI media. *Journal of Seismic Exploration*, 24: 231-257.

In this study, we introduce the unsplit Perfectly Matched Layer (PML) for the 2D and 3D second-order elastic wave equations with isotropic and transversely isotropic vertical axis of symmetry (VTI) media in the time domain. The introduced PML formulations are successfully applied to practical applications in terms of efficiency and stability. The PML formulations require less than or an equal number of auxiliary variables than other formulations, thereby decreasing the computational power necessary to calculate the solution in the PML zone. Derived directly from the second-order wave form, the PML formulation demonstrates an improved stability compared to first-order PMLs or second-order PMLs that are derived from first-order systems. Numerical examples demonstrate that the bulk waves and strong surface waves are perfectly damped out without introducing instability for an isotropic material in both 2D and 3D. The derived formulation also provides effective absorption with strong VTI materials, including zinc and apatite, that cause instability problems in other PML formulations.

KEY WORDS: perfectly matched layer, time-domain seismic wave modeling, second-order elastic wave equation, VTI media.

INTRODUCTION

Absorbing boundary conditions (ABCs) terminate undesired waves reflected from edges of a computational domain. As a result of the absorbing boundary, we can confine the domain within the zone of interest to perform numerical modeling of unbounded media. A perfectly matched layer is an absorbing boundary, introduced by Berenger (1994), and is known as the most

0963-0651/15/$5.00

effective of such boundary condition. The PML can damp out waves within a layer with a thickness of tens of nodes regardless of the frequency and incidence angle. Because of the successful results obtained for the electromagnetic wave problems, this technique was extended to other topics, including acoustic wave equations (Liu and Tao, 1997; Qi and Geers, 1997) and elastic wave equations (Hastings et al., 1995; Chew and Liu, 1996; Collino and Tsogka, 2001). However, instabilities have been reported whereby the wave solution can diverge exponentially in the PML layer (Abarbanel and Gottlib, 1997; Teixeira and Chew, 1999; Abarbanel et al., 2002), and an unconditionally stable PML formulation has yet to be presented.

Komatitsch and Tromp (2003) applied the original (split) PML to the second-order elastic wave equation that is represented with displacement wavefields. Most PML formulations have been applied to the first-order system of equations because it is easy to implement. However, from a practical point of view, the PML with the system of second-order wave equations has various advantages, including requiring fewer variables and its direct applicability to both standard finite-element-based methods and finite difference methods. In addition, the second-order wave equation has been commonly utilized in seismic data processing techniques such as full waveform inversion (Tarantola, 1986; Mora, 1987; Crase et al., 1990; Pratt et al., 1998; Shin and Cha, 2008; Shin and Cha, 2009) and reverse time migration (Chang and McMechan, 1987; Sun and McMechan, 2001; Yan and Sava, 2008; Kim et al., 2011).

Li and Matar (2010) applied the convolutional PML (CPML) to the second-order elastic wave equation that is derived from the first-order CPML proposed by Komatitsch and Martin (2007). It is noted that second-order CPMLs introduce large numbers of auxiliary variables and lead to instability problem with VTI media violating the geometric stability condition (Bécache et al., 2003). Recently, Assi and Cobbold (2013) derived unsplit PML from the first-order PML system, which requires only four auxiliary variables. However, the instability problem still occurred because this PML is basically the same as the first-order PML, and the stability problems proposed by Bécache et al. (2003) are inherent to both algorithms.

Duru and Kreiss (2012) suggested a PML formulation that is directly derived from the second-order wave equation. The authors verified that their formulation produces an extremely stable solution compared to the conventional first-order PML system even for VTI materials violating the geometric stability condition. However, this PML formulation requires twelve auxiliary variables even for the 2D elastic problem.

In this paper, we introduce the unsplit PML for the 2D and 3D second-order elastic wave equations with isotropic and VTI media in the time domain. This PML exhibits the stability of the PML of Duru and Kreiss (2012)

and also requires fewer auxiliary variables compared to the PML of Assi and Cobbold (2013). We begin by providing a detailed derivation of the second-order elastic PML system for 2D VTI media. Then, we extend the formulation to 3D media. Through numerical examples, the damping efficiency and stability of our PML formulation are demonstrated for isotropic materials and strong VTI media in the 2D domain. We also demonstrate the efficacy of MPML (Meza-Fajardo and Papageorgiou, 2008) in the case of instability for VTI materials significantly violating the geometric condition. Finally, we present numerical examples of the PML extended to the 3D domain with the same materials as in the 2D cases, which also demonstrate the efficiency and stability of the formulation. The finite difference method, which is second-order accurate in time and fourth-order accurate in space, is used for both the 2D and 3D simulations.

ELASTIC WAVE EQUATION

Linear particle motion in elastic media can be represented using the momentum conservation law as follows:

$$\rho(\partial^2\mathbf{u}/\partial t^2) = \nabla\cdot\boldsymbol{\sigma} + \mathbf{f} \ , \tag{1}$$

where ρ is the density and $\mathbf{u}$ is the displacement vector. This equation states that the net force on an infinitesimal volume is the summation of variations in the stress field $\boldsymbol{\sigma}$ and external force $\mathbf{f}$. A generalized Hooke's law relates the stress $\boldsymbol{\sigma}$ and strain $\boldsymbol{\varepsilon}$ to the stiffness tensor C, which determines the characteristics of the elastic media.

$$\boldsymbol{\sigma} = \mathrm{C}:\boldsymbol{\varepsilon} \ . \tag{2}$$

The stiffness tensor for transversely isotropic media with a vertical symmetry axis is expressed as (Thomsen, 1986)

$$\mathrm{C} = \begin{pmatrix} c_{11} & c_{12} & c_{13} & 0 & 0 & 0 \\ c_{12} & c_{11} & c_{13} & 0 & 0 & 0 \\ c_{13} & c_{13} & c_{33} & 0 & 0 & 0 \\ 0 & 0 & 0 & c_{44} & 0 & 0 \\ 0 & 0 & 0 & 0 & c_{44} & 0 \\ 0 & 0 & 0 & 0 & 0 & c_{44} \end{pmatrix} , \tag{3}$$

where $c_{66} = (c_{11} - c_{12})/2$. For the 2D problem in the x-z plane, the stiffness tensor can be reduced as follows:

$$C = \begin{pmatrix} c_{11} & c_{13} & 0 \\ c_{13} & c_{33} & 0 \\ 0 & 0 & c_{44} \end{pmatrix} . \tag{4}$$

For isotropic media, the stiffness tensor is composed of the Lamé parameters λ and μ. The stiffness tensor parameters are replaced as follows: $c_{11} = c_{33} = \lambda + 2\mu$, $c_{13} = \lambda$ and $c_{44} = \mu$. The strain tensor $\boldsymbol{\varepsilon}$ is then represented in terms of the displacement field as follows:

$$\boldsymbol{\varepsilon} = \tfrac{1}{2}(\nabla \mathbf{u} + \nabla \mathbf{u}^{T}) . \tag{5}$$

The above equations can be rewritten as the second-order elastic wave equation with respect to the displacement vector. The second-order elastic wave equation for VTI media in the 2D domain is

$$\rho(\partial^2 u/\partial t^2) = (\partial/\partial x)[c_{11}(\partial u/\partial x) + c_{13}(\partial w/\partial z)] + (\partial/\partial z)[c_{44}(\partial u/\partial z) + c_{44}(\partial w/\partial x)] + f_x , \tag{6a}$$

$$\rho(\partial^2 w/\partial t^2) = (\partial/\partial x)[c_{44}(\partial u/\partial z) + c_{44}(\partial w/\partial x)] + (\partial/\partial z)[c_{13}(\partial u/\partial x) + c_{33}(\partial w/\partial z)] + f_z . \tag{6b}$$

Many numerical techniques, such as the finite difference method (Marfurt, 1984; Appelö and Peterson, 2009), finite-element-based methods (Marfurt, 1984; Komatitsch and Vilotte, 1998; De Basabe et al., 2008; Min et al., 2003), and spectral- or pseudo-spectral-based methods (Carcione et al., 1988; Kosloff et al., 1989), have been used to solve this system. This study employs a finite difference method that is second-order accurate in time and fourth-order accurate in space.

PML FOR THE 2D ELASTIC WAVE EQUATION

A complex coordinate transformation is the basis of the PML suggested by Chew and Weedon (1994). The complex coordinate transformation is applied to the Helmholtz-like equations, which can be obtained by casting the wave equation in the frequency domain or the Laplace domain. In this study, the formulation in the Laplace domain is used in the PML zone. The complex stretched transformations in the 2D Cartesian coordinates are presented as

follows:

$$\tilde{x} = \int_0^x s_x(x')dx' = 1 + \int_0^x d_x(x')dx' \quad , \tag{7a}$$

$$\tilde{z} = \int_0^z s_z(z')dz' = 1 + \int_0^z d_z(z')dz' \quad , \tag{7b}$$

The damping profiles d_x and d_z should be positive in the PML zone and undefined or zero in a normal domain. The Helmholtz system of eqs. (6) is transformed with respect to the complex coordinate as follows:

$$\rho s^2\hat{u} = (\partial/\partial\tilde{x})[c_{11}(\partial\hat{u}/\partial\tilde{x}) + c_{13}(\partial\hat{w}/\partial\tilde{z})] + (\partial/\partial\tilde{z})[c_{44}(\partial\hat{u}/\partial\tilde{z}) + c_{44}(\partial\hat{w}/\partial\tilde{x})] \quad , \tag{8a}$$

$$\rho s^2\hat{w} = (\partial/\partial\tilde{x})[c_{44}(\partial\hat{u}/\partial\tilde{z}) + c_{44}(\partial\hat{w}/\partial\tilde{x})] + (\partial/\partial\tilde{z})[c_{13}(\partial\hat{u}/\partial\tilde{x}) + c_{33}(\partial\hat{w}/\partial\tilde{z})] \quad , \tag{8b}$$

where $\hat{u}$ and $\hat{w}$ are the horizontal and vertical displacement in the Laplace domain, respectively. The partial derivatives with respect to the stretched coordinates in the PML zone can be replaced by those of physical coordinates in the normal domain as follows:

$$\partial/\partial\tilde{x} = (1/s_x)(\partial/\partial x') \quad , \quad \partial/\partial\tilde{z} = (1/s_z)(\partial/\partial z) \quad , \tag{9}$$

where

$$s_x = 1 + d_x/s \quad , \quad s_z = 1 + d_z/s \quad . \tag{10}$$

Then, we can derive eq. (11) by substituting eq. (9) into (8), the PML formulation for the 2D elastic wave equation in the Laplace domain.

$$\rho s^2 s_x s_z\hat{u} = (\partial/\partial x)[c_{11}(s_z/s_x)(\partial\hat{u}/\partial x) + c_{13}(\partial\hat{w}/\partial z)] + (\partial/\partial z)[c_{44}(s_x/s_z)(\partial\hat{u}/\partial z) + c_{44}(\partial\hat{w}/\partial x)] \quad , \tag{11a}$$

$$\rho s^2 s_x s_z\hat{w} = (\partial/\partial x)[c_{44}(\partial\hat{u}/\partial z) + c_{44}(s_z/s_x)(\partial\hat{w}/\partial x)] + (\partial/\partial z)[c_{13}(\partial\hat{u}/\partial x) + c_{33}(s_x/s_z)(\partial\hat{w}/\partial z)] \quad . \tag{11b}$$

The wave solution in the Laplace or Fourier domain can be numerically obtained by an implicit method using an inverse matrix solver. The solutions

have been used for many seismic processing applications such as full waveform inversion in the frequency domain or Laplace domain (Pratt et al., 1998; Shin and Cha, 2008; Shin and Cha, 2009) and reverse time migration in the frequency domain (Kim, 2011).

Hereafter, we will take an inverse Laplace transform of eq. (11) to derive the PML in the time domain. The following time-domain PML formulation was applied to the acoustic wave equation by Grote and Sim (2010). Using the complex stretching parameter in eq. (10), eq. (11a) is written as

$$\rho[s^2\hat{u} + (d_x + d_z)s\hat{u} + d_xd_z\hat{u}]$$

$$= (\partial/\partial x)[c_{11}(\partial\hat{u}/\partial x) + \{c_{11}(d_z-d_x)/(s+d_x)\}(\partial\hat{u}/\partial x) + c_{13}(\partial\hat{w}/\partial z)]$$

$$+ (\partial/\partial z)[c_{44}(\partial\hat{u}/\partial z) + \{c_{44}(d_x-d_z)/(s+d_z)\}(\partial\hat{u}/\partial z) + c_{44}(\partial\hat{w}/\partial x)] \quad . \quad (12)$$

We can introduce the auxiliary variables $\hat{\phi}_{u,x}$ and $\hat{\phi}_{u,z}$ as follows:

$$\hat{\phi}_{u,x} = [c_{11}(d_z - d_x)/(s + d_x)](\partial\hat{u}/\partial x) \quad , \quad (13a)$$

$$\hat{\phi}_{u,z} = [c_{44}(d_x - d_z)/(s + d_z)](\partial\hat{u}/\partial z) \quad , \quad (13b)$$

or

$$s\hat{\phi}_{u,x} = -d_x\hat{\phi}_{u,x} + c_{11}(d_z - d_x)(\partial\hat{u}/\partial x) \quad , \quad (14a)$$

$$s\hat{\phi}_{u,z} = -d_z\hat{\phi}_{u,z} + c_{44}(d_x - d_z)(\partial\hat{u}/\partial z) \quad . \quad (14b)$$

Eq. (11b) can be reformulated in the same manner by introducing the auxiliary variables $\hat{\phi}_{w,x}$ and $\hat{\phi}_{w,z}$. The final form of the 2D PML formulation of the elastic wave equation with respect to the time domain is

$$\rho(\partial^2u/\partial t^2) = (\partial/\partial x)[c_{11}(\partial u/\partial x) + \phi_{u,x} + c_{13}(\partial w/\partial z)]$$

$$+ (\partial/\partial z)[c_{44}(\partial u/\partial z) + \phi_{u,z} + c_{44}(\partial w/\partial x)]$$

$$- \rho(d_x + d_z)(\partial u/\partial t) - \rho d_xd_z)u \quad , \quad (15a)$$

$$\rho(\partial^2w/\partial t^2) = (\partial/\partial x)[c_{44}(\partial u/\partial z) + c_{44}(\partial w/\partial x) + \phi_{w,x}]$$

$$+ (\partial/\partial z)[c_{13}(\partial u/\partial z) + c_{33}(\partial w/\partial x) + \phi_{w,z}]$$

$$- \rho(d_x + d_z)(\partial w/\partial t) - \rho d_xd_z)w \quad , \quad (15b)$$

$$d\phi_{u,x}/dt = -d_x\phi_{u,x} + c_{11}(d_z - d_x)(\partial u/\partial x) \quad , \tag{15c}$$

$$d\phi_{u,z}/dt = -d_z\phi_{u,z} + c_{44}(d_x - d_z)(\partial u/\partial z) \quad , \tag{15d}$$

$$d\phi_{w,x}/dt = -d_x\phi_{w,x} + c_{44}(d_z - d_x)(\partial w/\partial x) \quad , \tag{15e}$$

$$d\phi_{w,z}/dt = -d_z\phi_{w,z} + c_{33}(d_x - d_z)(\partial w/\partial z) \quad . \tag{15f}$$

The differential equations with respect to the auxiliary variables, which are also called the auxiliary difference equations (ADEs), must be solved in the PML zone, thereby increasing the computation costs. There are four auxiliary variables in the derived PML, which is equivalent to the formulation suggested by Assi and Cobbold (2013), who used fewer variables than other existing formulations for the 2D problem. For the ADEs, we impose Dirichlet boundary conditions with values of zero because the auxiliary variables outside of the PML zone remain equal to zero during the time marching step.

PML FOR THE 3D ELASTIC WAVE EQUATION

In this section, we extend the PML formulation to the 3D case. Except when considering the y-component, the majority of this procedure is identical to that of the 2D problem. Starting from the Helmholtz system of 3D elastic wave equations, we can derive the PML formulation in the Laplace domain as follows:

$$\begin{aligned}\rho s^2 s_x s_y s_z \hat{u} = {} & (\partial/\partial x)[c_{11}(s_y s_z/s_x)(\partial \hat{u}/\partial x) + c_{12}s_z(\partial \hat{v}/\partial y) + c_{13}s_y(\partial \hat{w}/\partial z)] \\ & + (\partial/\partial y)[c_{66}(s_z s_x/s_y)(\partial \hat{u}/\partial y) + c_{66}s_z(\partial \hat{v}/\partial x)] \\ & + (\partial/\partial z)[c_{44}(s_x s_y/s_z)(\partial \hat{u}/\partial z) + c_{44}s_y(\partial \hat{w}/\partial x)] \quad , \end{aligned} \tag{16a}$$

$$\begin{aligned}\rho s^2 s_x s_y s_z \hat{v} = {} & (\partial/\partial x)[c_{66}s_z(\partial \hat{u}/\partial y) + c_{66}(s_y s_z/s_x)(\partial \hat{v}/\partial x)] \\ & + (\partial/\partial y)[c_{12}s_z(\partial \hat{u}/\partial x) + c_{11}(s_z s_x/s_y)(\partial \hat{v}/\partial y) + c_{13}s_x(\partial \hat{w}/\partial z)] \\ & + (\partial/\partial z)[c_{44}(s_x s_y/s_z)(\partial \hat{v}/\partial z) + c_{44}s_y(\partial \hat{w}/\partial x)] \quad , \end{aligned} \tag{16b}$$

$$\begin{aligned}\rho s^2 s_x s_y s_z \hat{w} = {} & (\partial/\partial x)[c_{44}s_y(\partial \hat{u}/\partial z) + c_{44}(s_y s_z/s_x)(\partial \hat{w}/\partial x)] \\ & + (\partial/\partial y)[c_{44}s_x(\partial \hat{v}/\partial z) + c_{44}(s_z s_x/s_y)(\partial \hat{w}/\partial y)] \\ & + (\partial/\partial z)[c_{13}s_y(\partial \hat{u}/\partial x) + c_{13}s_x(\partial \hat{v}/\partial y) + c_{33}(s_z s_x/s_y)(\partial \hat{w}/\partial z)] \quad . \end{aligned} \tag{16c}$$

Eq. (16a) is rewritten by substituting the complex stretch parameters s_x, s_y and

s_z as follows:

$$\rho[s^2\hat{u} + (d_x+d_y+d_z)s\hat{u} + (d_xd_y+d_yd_z+d_zd_x)\hat{u} + d_xd_yd_z(\hat{u}/s)]$$

$$= (\partial/\partial x)[c_{11}(\partial\hat{u}/\partial x) + c_{11}\{[(d_y+d_z-d_x)/(s+d_x)] + [d_yd_z/s(s+d_x)]\}(\partial\hat{u}/\partial x)$$

$$+ c_{12}(\partial\hat{v}/\partial y) + c_{12}(d_z/s)(\partial\hat{v}/\partial y) + c_{13}(\partial\hat{w}/\partial z) + c_{13}(d_y/s)(\partial\hat{w}/\partial z)$$

$$+ (\partial/\partial y)[c_{66}(\partial\hat{u}/\partial y) + c_{66}\{[(d_z+d_x-d_y)/(s+d_y)] + [d_zd_x/s(s+d_y)]\}(\partial\hat{u}/\partial y)$$

$$+ c_{66}(\partial\hat{v}/\partial x) + c_{66}(d_z/s)(\partial\hat{v}/\partial x)$$

$$+ (\partial/\partial z)[c_{44}(\partial\hat{u}/\partial z) + c_{44}\{[(d_x+d_y-d_z)/(s+d_z)] + [d_xd_y/s(s+d_z)]\}(\partial\hat{u}/\partial z)$$

$$+ c_{44}(\partial\hat{w}/\partial x) + c_{44}(d_y/s)(\partial\hat{w}/\partial x) \quad . \tag{17}$$

We can introduce new auxiliary variables $\hat{\varphi}_u$, $\hat{\varphi}_v$ and $\hat{\varphi}_w$

$$\hat{\varphi}_u = (1/s)\hat{u} \ , \quad \hat{\varphi}_v = (1/s)\hat{v} \ , \quad \hat{\varphi}_w = (1/s)\hat{w} \ . \tag{18}$$

On the right-hand side, the other auxiliary variables are defined as

$$\hat{\phi}_{u,x} = c_{11}\{[(d_y+d_z+d_x)/(s+d_x)] + [(d_yd_z)/s(s+d_x)]\}(\partial\hat{u}/\partial x) \ , \tag{19a}$$

$$\hat{\phi}_{u,y} = c_{66}\{[(d_z+d_x+d_y)/(s+d_y)] + [(d_zd_x)/s(s+d_y)]\}(\partial\hat{u}/\partial y) \ , \tag{19b}$$

$$\hat{\phi}_{u,z} = c_{44}\{[(d_x+d_y+d_z)/(s+d_z)] + [(d_xd_y)/s(s+d_z)]\}(\partial\hat{u}/\partial z) \ , \tag{19c}$$

or

$$s\hat{\phi}_{u,x} = -d_x\hat{\phi}_{u,x} + c_{11}[(d_y+d_z+d_x)(\partial\hat{u}/\partial x)] + [d_yd_z(\partial\hat{\phi}_u/\partial x) \ , \tag{20a}$$

$$s\hat{\phi}_{u,y} = -d_y\hat{\phi}_{u,y} + c_{66}[(d_z+d_x+d_y)(\partial\hat{u}/\partial y)] + [d_zd_x(\partial\hat{\phi}_u/\partial y) \ , \tag{20b}$$

$$s\hat{\phi}_{u,z} = -d_z\hat{\phi}_{u,z} + c_{44}[(d_x+d_y+d_z)(\partial\hat{u}/\partial z)] + [d_xd_y(\partial\hat{\phi}_u/\partial z) \ . \tag{20c}$$

The remainder of eq. (16) can be reformulated in the same manner by introducing $\hat{\phi}_{v,x}$, $\hat{\phi}_{v,y}$, $\hat{\phi}_{v,z}$, $\hat{\phi}_{w,x}$, $\hat{\phi}_{w,y}$ and $\hat{\phi}_{w,z}$. The final formulation of the PML is presented in the Appendix. As in the 2D case, the number of auxiliary variables introduced is less than or equal to those of other formulations. Table 1 illustrates the number of auxiliary variables required for the PML formulation of the second-order elastic wave equation for both the 2D and 3D cases. There are fewer auxiliary variables in the derived PML formulation than in the CPML and the original PML (half and two thirds as many variables for the 2D and 3D cases, respectively).

Table 1. Number of auxiliary variables needed for the derived PML, CPML and original PML for both the 2D and 3D formulations.

	Derived PML	CPML	Original PML
2D Elastic	4	8	8
3D Elastic	2	18	18

NUMERICAL EXAMPLES

In this section, we demonstrate the absorbing behavior of the PML proposed in the previous section. We perform numerical tests with isotropic and VTI media. Fig. 1 illustrates the computational domain of the numerical test.

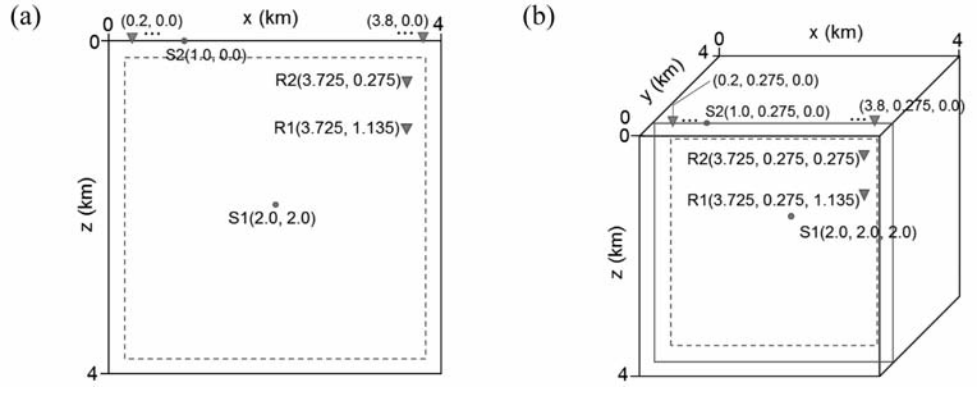

Fig. 1. Computational domain of the (a) 2D plane and (b) the 3D cube.

For the 2D problem, we utilized a 4x4-km square domain with a 120-m thick PML layer surrounding the domain. We impose a source at S1(2.0, 2.0) to simulate bulk waves. Bulk wave signals are received at R1(3.725, 1.135) and R2(3.725, 0.275) in the 2D domain. To simulate the surface wave in the half-infinite domain, we impose a source at S2(1.0, 0.0) and receivers (inverted triangles) at the surface form (0.2, 0.0) to (3.8, 0.0), as shown in Fig. 1a. In this case, we set a free stress boundary condition at the top surface instead of the PML layer.

For the 3D problem, a cube with dimensions of 4x4x4 km is utilized as the computational domain with a 120-m thick PML layer for all of the outer surfaces. We place the source at S1(2.0, 2.0, 2.0) to simulate the bulk waves, which are recorded at R1(3.725, 0.275, 1.135) and R2(3.725, 0.275, 0.275). We also simulate the surface waves for the 3D domain with source (S2) and receivers from (0.2, 0.275, 0.0) to (3.8, 0.275, 0.0) at the surface, as shown in Fig. 1b. Similarly to the 2D case, we utilize a free stress boundary condition at the top surface.

The damping profile d_x in the PML layer for the x-direction, which starts from x_0 and has a thickness L_x, is set as a quadratic function as follows:

$$d_x = d_{max}[(x - x_0)/L_x]^2 \quad , \tag{21}$$

where

$$d_{max} = -v_{max}\log R/2L_x \quad . \tag{22}$$

R is the reflection coefficient, which is set to 10^{-3} in the numerical tests. The damping profiles in the y- and z-directions are applied to the PML layer in the same manner.

2D ISOTROPIC MEDIA

We applied the PML to 2D isotropic media with a density $\rho = 2000$ kg/m^3 and Lamé constants $\lambda = 1.496 \times 10^9$ N/m^2 and $\mu = 1.507 \times 10^9$ N/m^2. A source is imposed, in the z-direction, as a time derivative of the Gaussian function as follows:

$$q(t) = -(\sqrt{2})\pi f_0(t - t_0)e^{-\pi^2 f_0^2(t-t_0)} \quad , \tag{23}$$

where f_0 is the peak frequency and t_0 is the delay time. In this case, we use $f_0 = 20$ Hz and $t_0 = 0.45$ s.

Fig. 2 shows 2D snapshots of the vertical displacement (w) in the bulk wave simulation at four different times of up to 20 s in the modeling. The snapshots illustrate the wave propagating in the 2D plane and the P-wave entering into the PML layer followed by the S-wave. Both of the waves are clearly damped out without generating reflections. To distinguish reflections from the wavefield, we generated an analytical solution using a much larger computational domain. A comparison of the time evolution of the horizontal and vertical displacements (w) at the receiver locations in the model in Fig. 1a to the analytic solution demonstrates that significant reflections are not visible from the PML zone, as shown in Fig. 3.

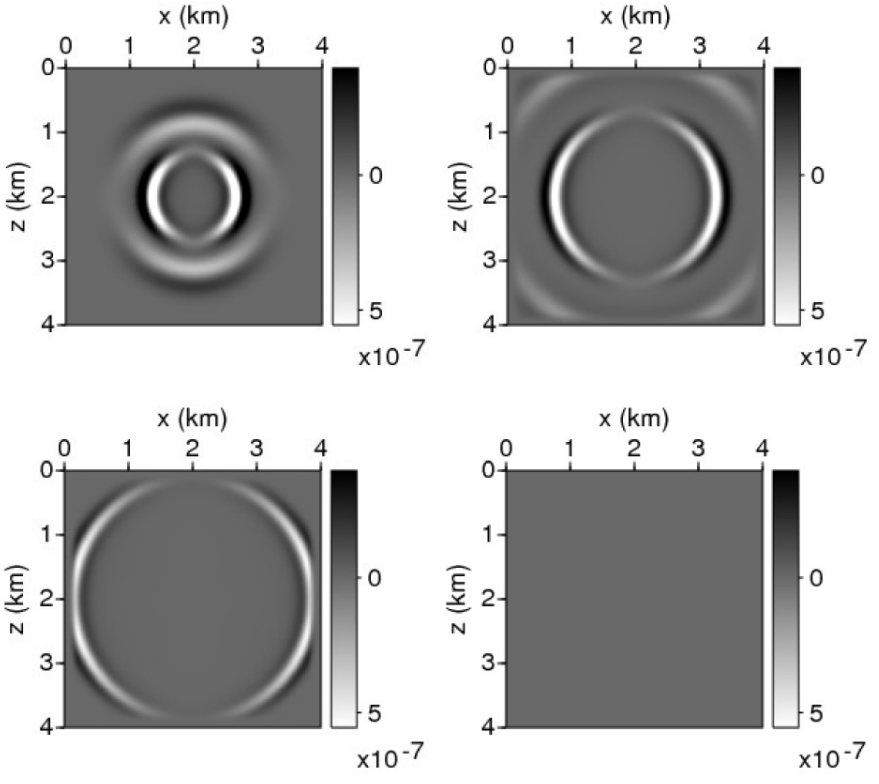

Fig. 2. Snapshots of the vertical displacement of bulk waves in the 2D isotropic media. The snapshots are at t = 0.7 s, t = 1.05 s, t = 0.75 s, and t = 20 s.

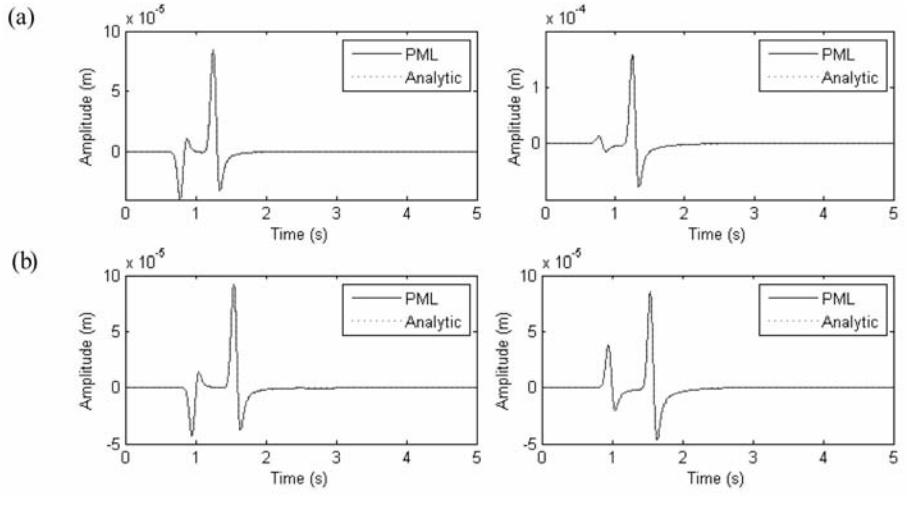

Fig. 3. (a) Time evolution of horizontal displacement (left) and vertical displacement (right) at R1 compared to analytic trace. (b) Time evolution of horizontal displacement (left) and vertical displacement (right) at R2 compared to analytic trace.

Late time instability, a blow-up phenomenon that can occur after quiescence, has been reported with the use of the unsplit PML (Abarbanel et al., 2002). The total mechanical energy of the computational domain, excluding the PML layer, is calculated to detect the instability during the modeling as follows:

$$E = \int_{\Omega} (\tfrac{1}{2}\rho \| v \|^2 + \tfrac{1}{2}\sigma_{ij}\varepsilon_{ij}) d\Omega \quad . \tag{24}$$

Fig. 4 illustrates the mechanical energy in the normal domain and shows that the energy of the P-waves decays at approximately t = 2.5 s and that the energy of the S-waves decays at approximately t = 6.6 s. The total energy gradually decreases, and no instability is visible up to 100 s.

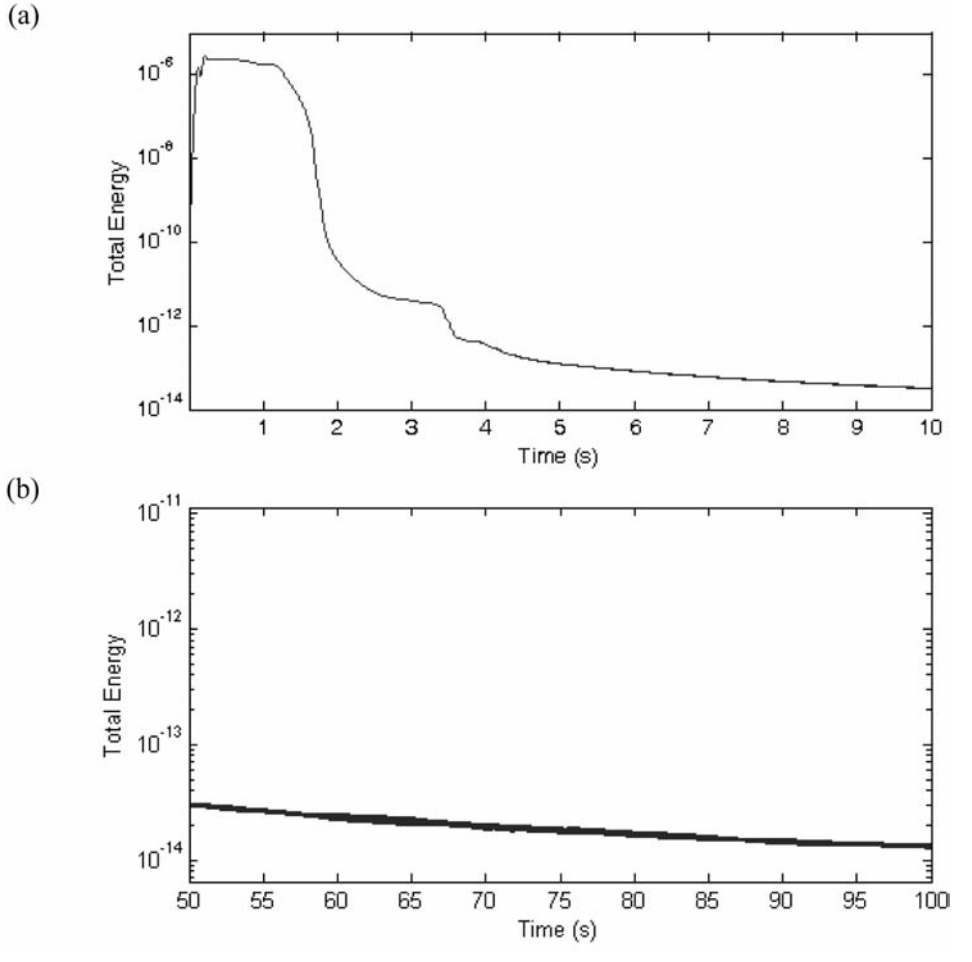

Fig. 4. (a) Mechanical energy history in the normal domain from 0 to 10 s and (b) from 50 to 100s using a log scale for the 2D elastic wave propagation.

We also performed the wave propagation modeling in the half-infinite elastic media to simulate surface waves at the top boundary. Fig. 5 illustrates a seismogram of the vertical displacement (w) up to 20 s and shows that P-wave and Rayleigh waves are clearly damped out without significant reflections from the PML layer.

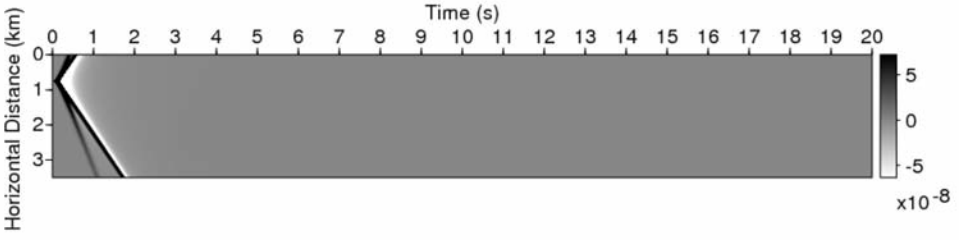

Fig. 5. Seismogram of vertical displacement for the 2D isotropic media up to 20 s.

2D VTI MEDIA

For the numerical test with the 2D VTI media, we use VTI materials having strong Thomsen parameters such as shale, muscovite, biotite, calcite, apatite and zinc (Ledbetter, 1977; Thomsen, 1986). The properties of the materials are presented in Table 2. The stability of the PML with VTI materials depends on the material properties, and Bécache et al. (2003) proposed the necessary stability condition, which is called the geometric stability condition because it means that the projection of the slowness vector to the group velocity

Table 2. Stiffness parameters of strong VTI materials for the numerical examples presented in Thomsen (1986) and Ledbetter (1977). Calcite, apatite and zinc violate the geometric stability condition (Bécache et al., 2003).

	ρ(g/cm^3)	c_{12}(GPa)	c_{11}(GPa)	c_{13}(GPa)	c_{33}(GPa)	c_{44}(GPa)	c_{66}(GPa)
Shale	2.42	38.64	16.93	14.68	27.6	5.37	10.85
Muscovite	2.28	144.32	33.47	11.75	44.54	9.97	55.43
Biotite	3.05	172.64	27.4	10.53	50.13	5.48	72.62
Calcite	2.71	134.01	52.48	49.15	77.1	30.47	40.77
Apatite	3.2	153.58	10.82	59.12	128.63	61.64	71.38
Zinc	7.1	163	30.6	48.1	60.3	39.4	65.9

vector must be in the same direction. The relation between the group velocity direction ϕ and slowness direction θ was presented in Thomsen (1986) as follows:

$$\begin{aligned} \tan\phi_P &= \tan\phi_P[1 + 2\delta + 4(\varepsilon - \delta)\sin^2\theta_P] \quad , \\ \tan\phi_{SV} &= \tan\theta_{SV}[1 + 2(\alpha_0^2/\beta_0^2)(\varepsilon - \delta)(1 - \sin^2\theta_{SV})] \quad , \\ \tan\phi_{SH} &= \tan\phi_{SH}(1 + 2\gamma) \quad , \end{aligned} \tag{25}$$

where α_0 and β_0 are P- and S-wave speeds, respectively, in the vertical direction and ε, δ and γ are Thomsen parameters. For weakly anisotropic VTI materials, which have Thomsen parameters $\varepsilon \ll 1$, $\delta \ll 1$ and $\gamma \ll 1$, the direction of the slowness vector and the group velocity are almost equal, and the solution is stable in the PML layer, thus satisfying the geometric stability condition. However, strong VTI materials, such as calcite, apatite, and zinc crystal, which are listed in Table 2, can easily violate the stability condition. For this reason, the exponential blow-up problem is typically considered using a PML formulation such as the CPML (Komatitsch and Martin, 2007; Li and Matar, 2010) or the unsplit PML (Assi and Cobbold, 2013).

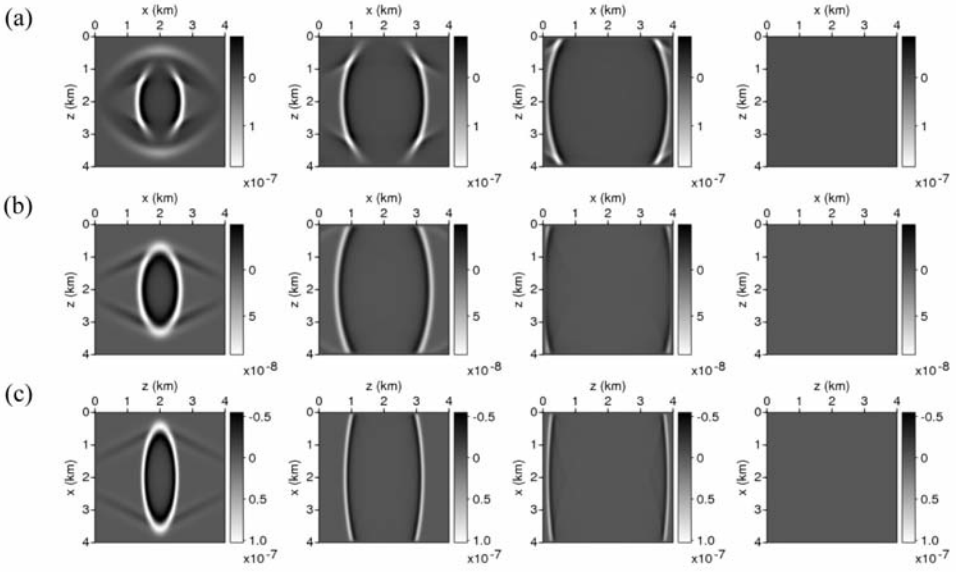

Fig. 6. Snapshots of the vertical displacement of a bulk wave in the 2D VTI media. (a) Snapshots at t = 0.6 s, t = 1 s, t = 1.4 s, and t = 20 s for shale. (b) Snapshots at t = 0.4 s, t = 0.75 s, t = 1.05 s, and t = 20 s, , and for muscovite. (c) Snapshots at t = 0.5 s, t = 1 s, t = 1.5 s, and t = 20 s for biotite.

For the wavelet, we use the time derivative of the Gaussian function, eq. (21), and apply it in the negative z-direction with $f_0 = 17$ Hz and $t_0 = 0.14$ s for shale, muscovite, and biotite and with $f_0 = 30$ Hz and $t_0 = 0.08$ s for calcite, apatite, quartz and zinc crystal. Figs. 6 and 7 illustrate snapshots of the propagation of the vertical displacement (w) in the bulk wave modeling at four different times for the VTI materials in Table 2. The snapshots illustrate the propagation of the quasi-p- and quasi-s-waves, which are clearly damped out in the PML layer without instabilities for up to 20 s for most of the materials. The PML does not lead to instabilities for calcite, apatite, and zinc, which are materials that violate the geometric condition. We also generated a synthetic seismogram with the half-infinite media using the stress-free boundary condition at the top surface. The seismograms of the vertical displacement (w) for the materials in Table 2 are presented in Figs. 8 and 9. Likewise, for the bulk waves illustrated in Figs. 5 and 6, the PML layer does not yield significant reflections and instability up to 20 s of simulation for the surface waves.

However, instability does occur for the materials significantly violating the geometric stability condition, such as the material used in Bécache et al. (2003) with $c_{11} = 4 \times 10^9$ N/m^2, $c_{33} = 20 \times 10^9$ N/m^2, $c_{44} = 2 \times 10^9$ N/m^2,

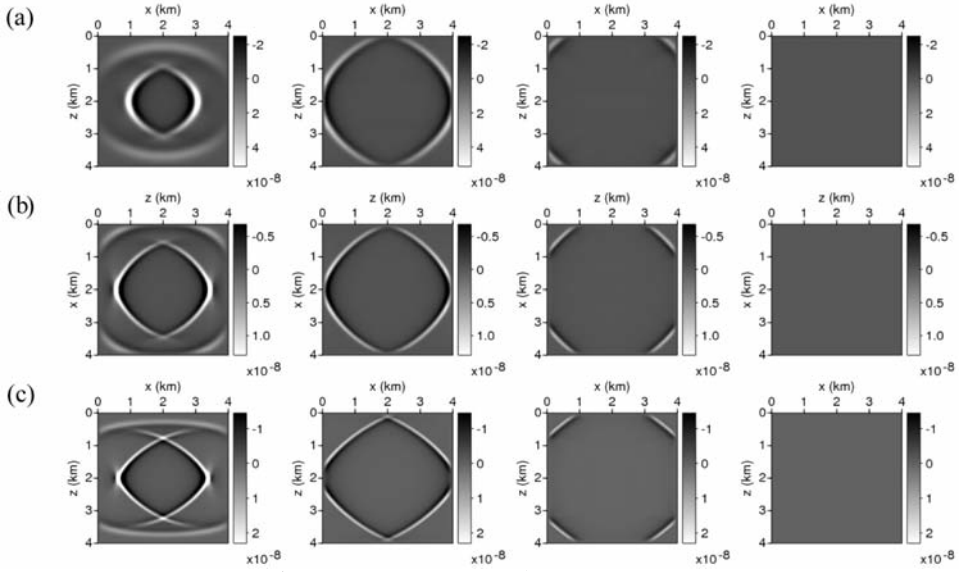

Fig. 7. Snapshots of the vertical displacement of a bulk wave in 2D VTI media violating the geometric stability condition. (a) Snapshots at t = 0.3 s, t = 0.6 s, t = 0.85 s, and t = 20 s for calcite. (b) Snapshots at t = 0.3 s, t = 0.525 s, t = 0.75 s, and t = 20 s for apatite. (c) Snapshots at t = 0.5 s, t = 1 s, t = 1.5 s, and t = 20 s for zinc.

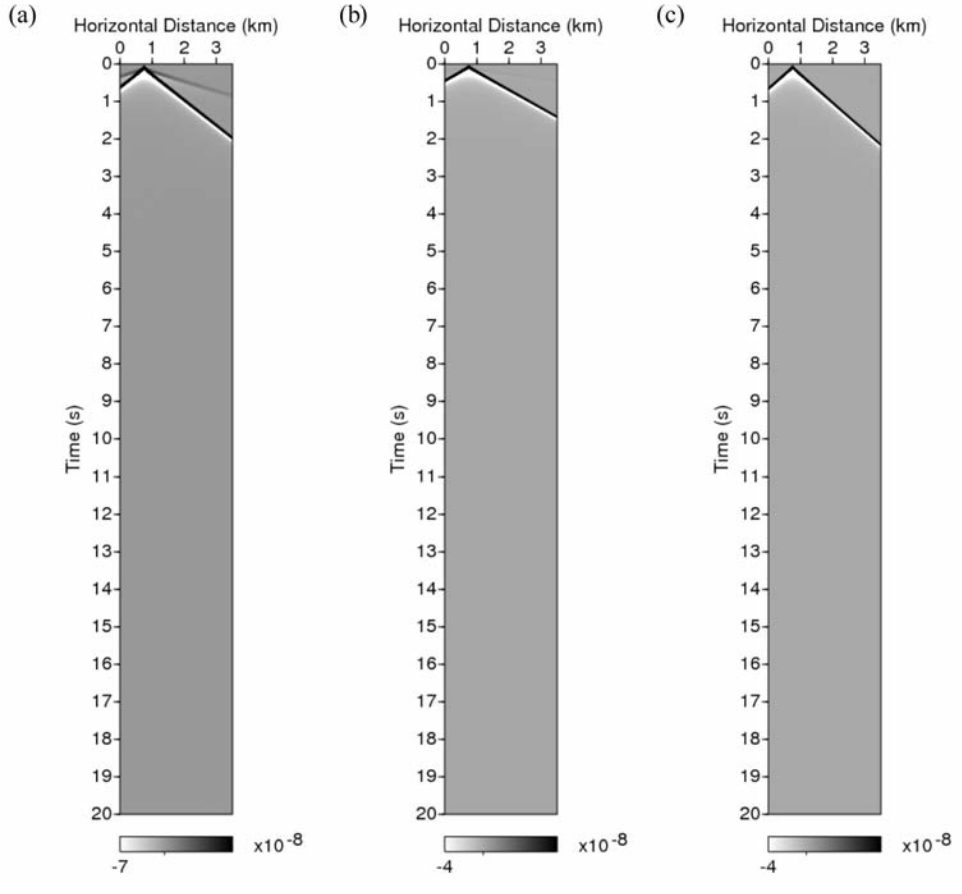

Fig. 8. Seismogram of vertical displacement for the 2D VTI media up to 20 s. (a) Shale. (b) Muscovite. (c) Biotite.

$c_{13} = 7.5 \times 10^9$ N/m^2 and $\rho = 1000$ kg/m^3, which exhibits the instability problem under most types of PML formulations. In the early stage, the instability starts at the entrance of the PML zone and spreads along the layer, as presented at the top of Fig. 10a. The instability can be mitigated using the MPML suggested by Meza-Fajardo and Papageorgiou (2008), which is a simple technique that uses the sponge boundary effect in the PML zone. Fig. 10b shows snapshots of the wave propagation using the MPML. No instabilities are visible in this case; however, long-wavelength reflections are observed because of the sponge layer effect.

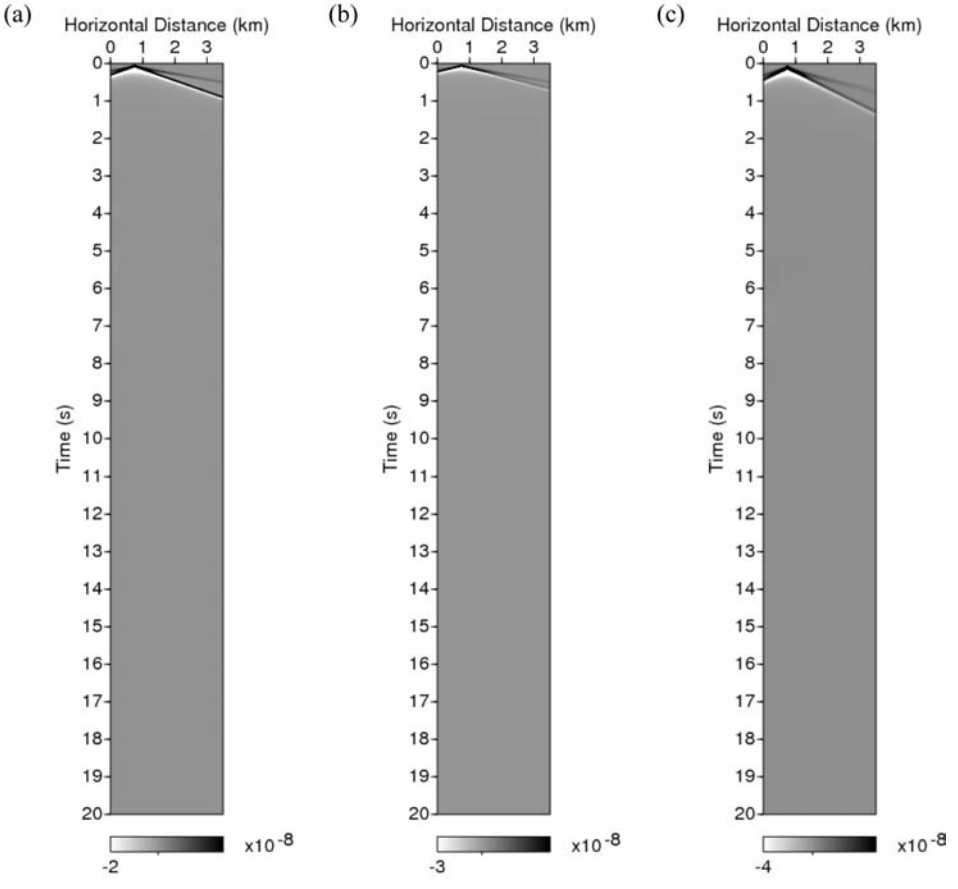

Fig. 9. Seismogram of vertical displacement for the 2D VTI media violating the geometric stability condition up to 20 s. (a) Calcite. (b) Apatite. (c) Zinc.

3D ISOTROPIC MEDIA

We applied the PML to 3D isotropic media with a density $\rho = 2000$ kg/m^3, and Lamé constants of $\lambda = 1.496 \times 10^9$ N/m^2 and $\mu = 1.507 \times 10^9$ N/m^2. The source wavelet is imposed in the z-direction with the time derivative of the Gaussian function with $f_0 = 10$ Hz and $t_0 = 0.45$ s.

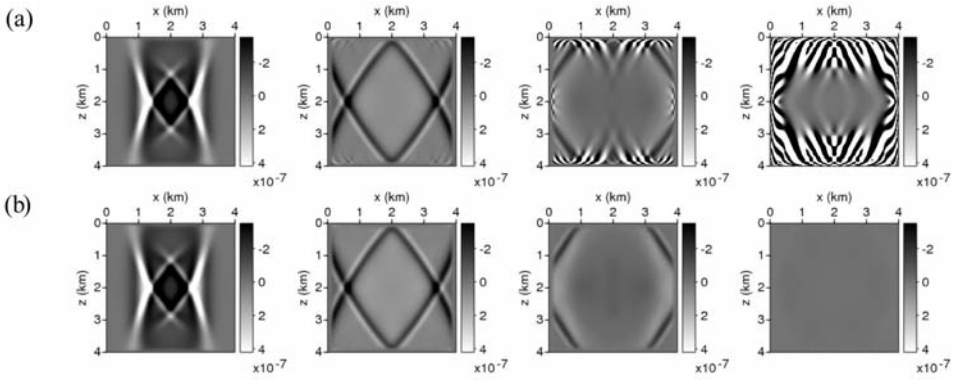

Fig. 10. (a) Snapshots of the vertical displacement of bulk waves at t = 1 s, t = 2 s, t = 3 s, and t = 20 s for the material introduced by Bécache et al. (2003) violating the geometric stability condition, which yields instability. (b) Snapshots when the MPML is imposed on the PML layer.

Fig. 11 presents snapshots of the vertical displacement (w) in the bulk wave simulation at four different times for up to 20 s in the simulation. The results show that the PML is effective for 3D isotropic media in that no reflections from the boundaries are observed. Fig. 12 presents the time traces of the horizontal and vertical displacement (w) recorded at the receiver locations. Similar to the 2D isotropic media case, the analytic solution is obtained using the numerical solution with a larger media model; the solution is in good agreement with the numerical solution with the PML zone. The total mechanical energy is calculated in the computational domain, excluding the PML layer, and is presented in Fig. 13. The total mechanical energy gradually decreases, and no late-time instability is visible in the first 100 s of modeling.

We also performed numerical modeling of the half-infinite media to simulate surface waves in the 3D domain. Fig. 14 shows the synthetic seismogram of the vertical displacement (w) for the isotropic media, wherein the p-waves and Rayleigh waves are damped out in the PML layer.

3D VTI MEDIA

For the numerical test with the 3D VTI media, we use the materials presented in Table 2, which are utilized for the 2D numerical examples. Figs. 15 and 16 present snapshots of the vertical displacement (w) in the bulk wave modeling at four different times up to 20 s. The wavelets are the same as those in the 2D modeling case and are applied in the negative z-direction. The stability condition of the VTI media, and likewise for the geometric condition

in the 2D problem, is not explicitly presented for the PML with the 3D elastic wave equation. It is yet to be defined if the stability criterion is relaxed; the snapshots show that the bulk waves are effectively damped out in the PML layer without any instabilities for up to 20 s for all materials, including calcite, apatite and zinc, which violate the geometric condition in the 2D problem. Figs. 17 and 18 demonstrate that the surface waves are also effectively absorbed by the PML layer for the strong VTI media.

Despite the numerical results, we expect that instability may occur with VTI media as in the numerical example of the 2D case. For the 3D problem, we do not search for hypothetical materials that can cause the exponential blow-up phenomenon, and a mathematical analysis must be performed to understand the stability characteristics of the 3D elastic wave PML for VTI materials.

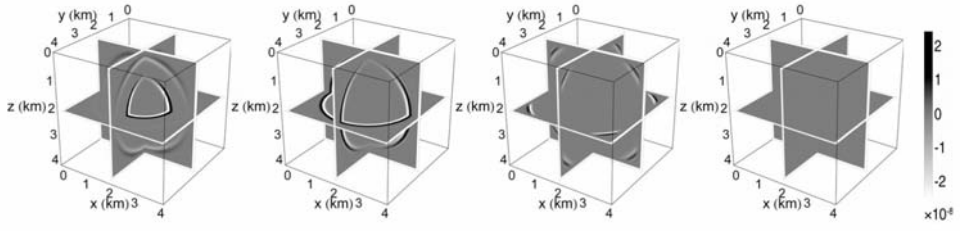

Fig. 11. Snapshots of the vertical displacement of a bulk wave in the 3D isotropic media. The snapshots are at t = 0.7 s, t = 1.05 s, t = 1.4 s, and t = 20 s.

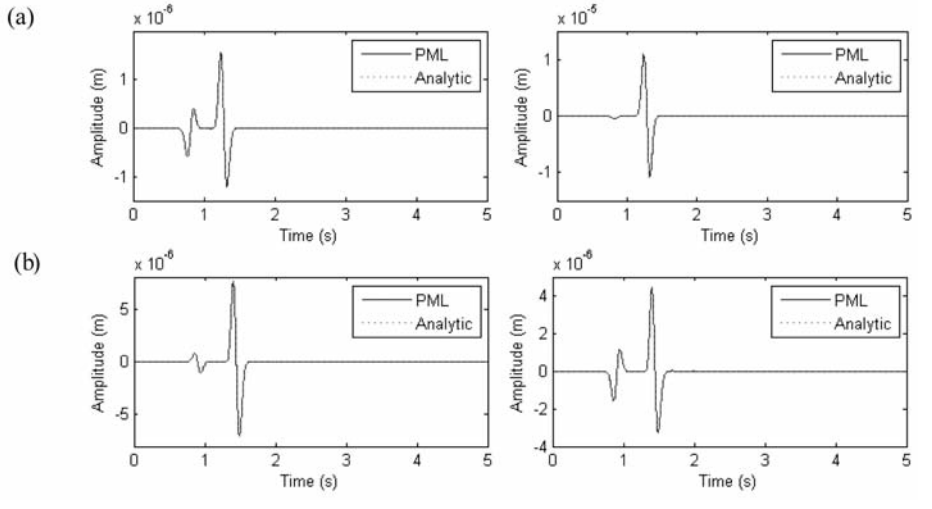

Fig. 12. (a) Time evolution of horizontal displacement (left) and vertical displacement (right) at R1 compared to analytic trace. (b) Time evolution of horizontal displacement (left) and vertical displacement (right) at R2 compared to analytic trace.

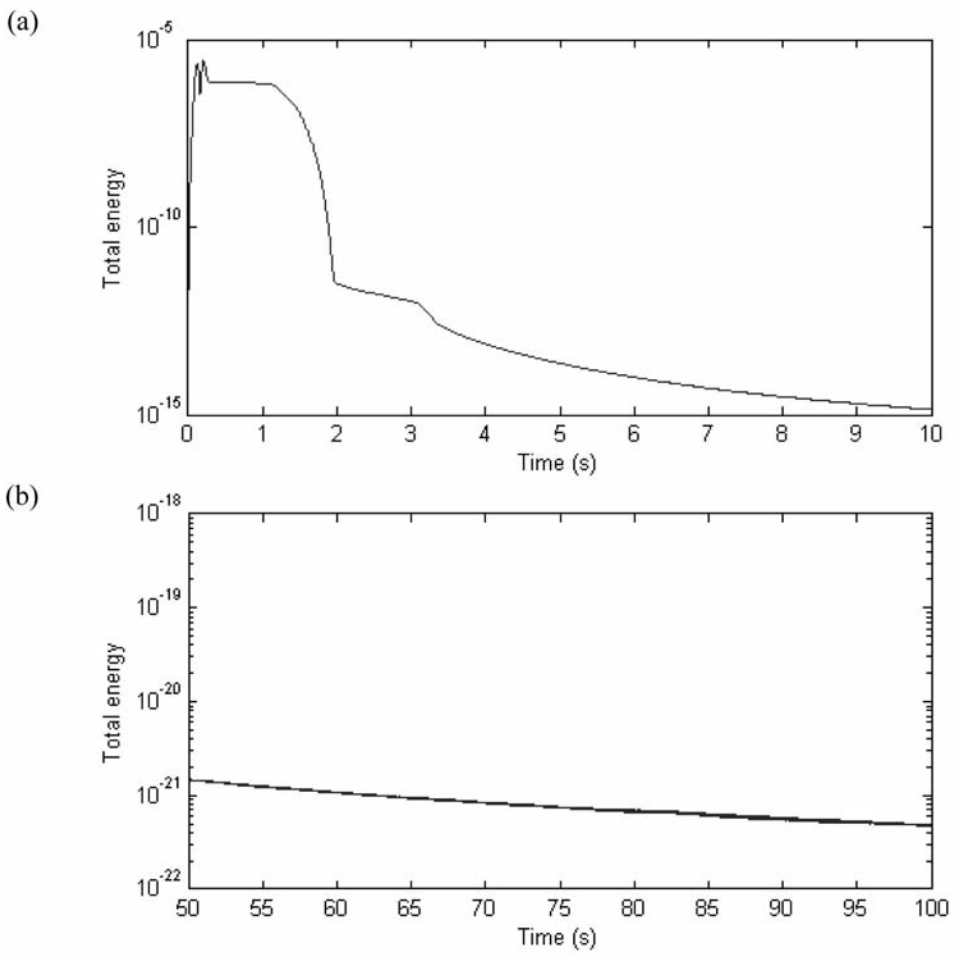

Fig. 13. (a) Mechanical energy history in the normal domain from 0 to 10 s and (b) from 50 to 100 s using a log scale for the 3D elastic wave propagation.

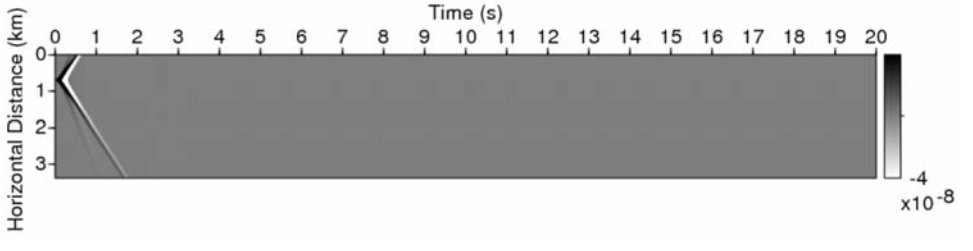

Fig. 14. Seismogram of vertical displacement for the 3D isotropic media up to 20 s.

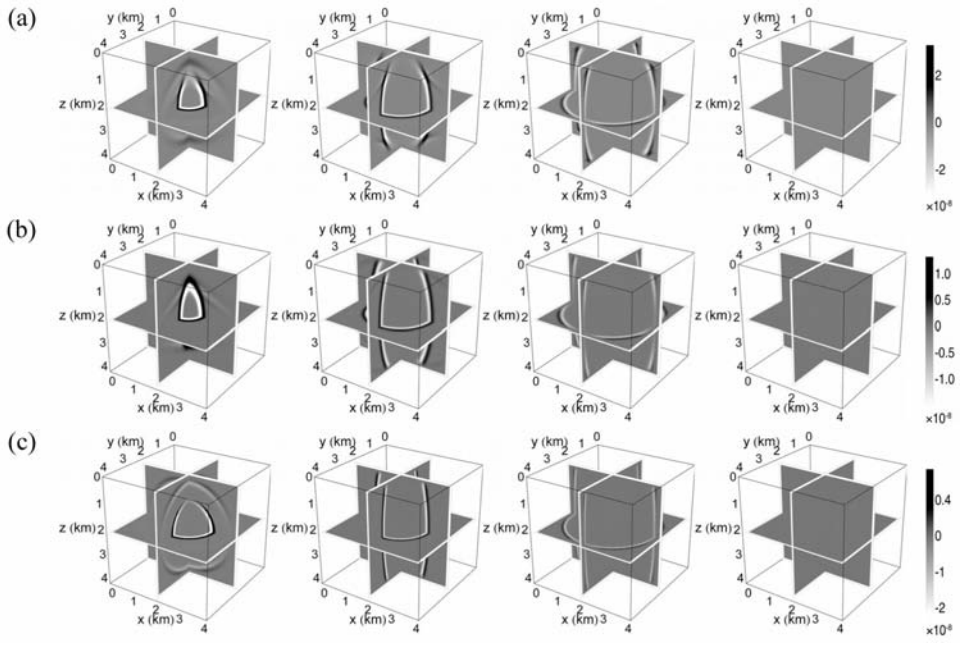

Fig. 15. Snapshots of the vertical displacement of bulk waves in the 3D VTI media. (a) Snapshots at t = 0.6 s, t = 1 s, t = 1.4 s, and t = 20 s for shale. (b) Snapshots at t = 0.4 s, t = 0.75 s, t = 1.05 s, and t = 20 s for muscovite. (c) Snapshots at t = 0.5 s, t = 1 s, t = 1.5 s, and t = 20s for biotite.

CONCLUSION

In this study, we introduced the time-domain PML formulation of the second-order elastic wave equation for isotropic and VTI media. The derived formulation requires a number of auxiliary variables. However, the formulation requires half and two thirds as many variables compared to the original PML or CPML for the 2D and 3D cases, respectively, thereby reducing the computational costs of solving the system in the PML zone. For isotropic media, the incoming waves are almost completely damped out in the PML zone without exhibiting instability or linear growth phenomena for up to 100 s of simulation. The PML layer also eliminated wavefields in the strong VTI media, which caused instability in other PML formulations. Our PML formulations are both efficient and stable, and the numerical examples demonstrated that the PML formulations are suitable for materials commonly found in practical

seismic problems. The PML formulations of other types of anisotropic materials, such as tilted transversely isotropic (TTI) or orthotropic media, need to be studied in the near future.

DATA AND RESOURCES

No data were used in this paper. The codes simulating 2D and 3D elastic wave propagation were developed by the authors and performed on a computer with an Intel 3.2 GHz processor to generate the results for the numerical examples.

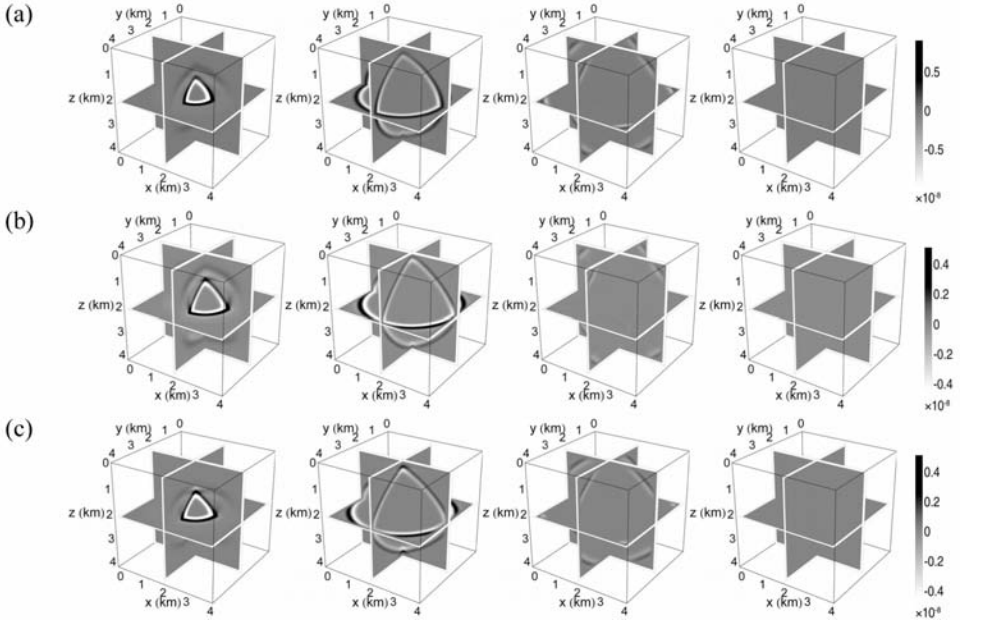

Fig. 16. Snapshots of the vertical displacement of bulk waves in the 3D VTI media violating the geometric stability condition. (a) Snapshots at t = 0.3 s, t = 0.6 s, t = 0.85 s, and t = 20 s for calcite. (b) Snapshots at t = 0.3 s, t = 0.525 s, t = 0.75 s, and t = 20 s for apatite. (c) Snapshots at t = 0.5 s, t = 1 s, t = 1.5 s, and t = 20 s for zinc.

ACKNOWLEDGMENTS

This work was supported by the Energy Efficiency & Resources Core Technology Program of the Korea Institute of Energy Technology Evaluation and Planning (KETEP) and granted financial resources from the Ministry of Trade, Industry & Energy, Republic of Korea. (No. 20132510100060)

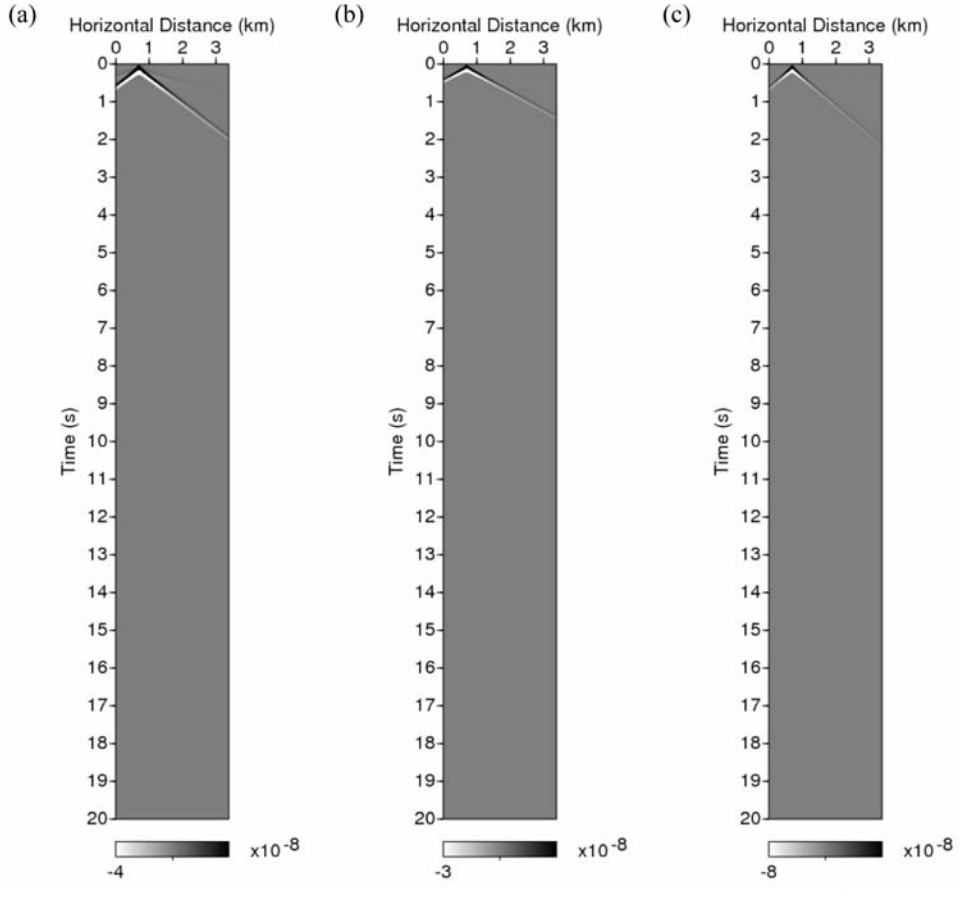

Fig. 17. Seismogram of vertical displacement for the 2D VTI media up to 20 s. (a) Shale. (b) Muscovite. (c) Biotite.

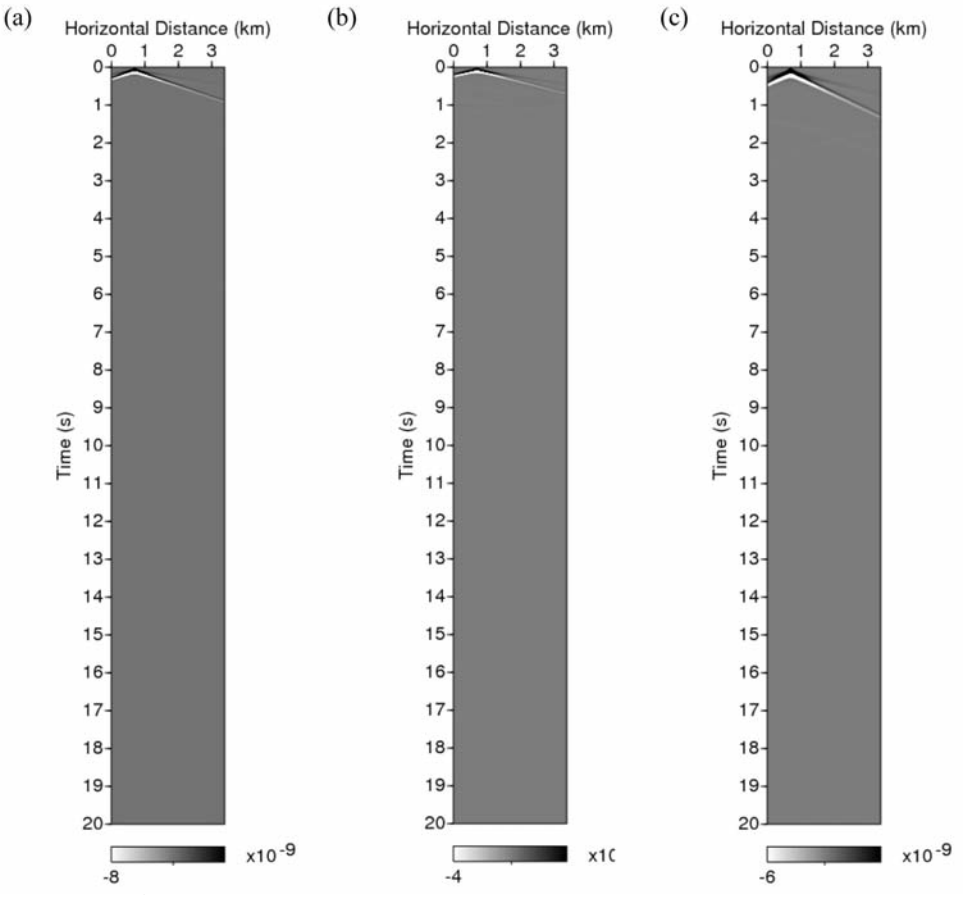

Fig. 18. Seismogram of vertical displacement for the 2D VTI media violating the geometric stability condition up to 20 s. (a) Calcite. (b) Apatite. (c) Zinc.

REFERENCES

Abarbanel, S. and Gottlieb, D., 1997. A mathematical analysis of the PML method. J. Computat. Phys., 134: 357-363.

Abarbanel, S., Gottlieb, D. and Hesthaven, J.S., 2002. Long time behavior of the perfectly matched layer equations in computational electromagnetics. J. Scientif. Comput., 17: 405-422.

Appelö, D. and Petersson, N.A., 2009. A stable finite difference method for the elastic wave equation on complex geometries with free surfaces. Communic. Computat. Phys., 5: 84-107.

Assi, H. and Cobbold, R.S., 2013. Perfectly matched layer for second-order time-domain elastic wave equation: formulation and stability. arXiv preprint arXiv: 1312.3722.

Bécache, E., Fauqueux, S. and Joly, P., 2003. Stability of perfectly matched layers, group velocities and anisotropic waves. J. Computat. Phys., 188: 399-433.

Berenger, J.P., 1994. A perfectly matched layer for the absorption of electromagnetic waves. J. Computat. Phys., 114: 185-200.

Carcione, J.M., Kosloff, D. and Kosloff, R., 1988. Wave-propagation simulation in an elastic anisotropic (transversely isotropic) solid. Quart. J. Mechan. Appl. Mathemat., 41: 319-346.

Chang, W.F. and McMechan, G.A., 1987. Elastic reverse-time migration. Geophysics, 52: 1365-1375.

Chew, W.C. and Liu, Q.H., 1996. Perfectly matched layers for elastodynamics: a new absorbing boundary condition. J. Computat. Acoust., 4: 341-359.

Chew, W.C. and Weedon, W.H., 1994. A 3D perfectly matched medium from modified Maxwell's equations with stretched coordinates. Microw. Opt. Technol. Lett., 7: 599-604.

Collino, F., and Tsogka, C., 2001. Application of the perfectly matched absorbing layer model to the linear elastodynamic problem in anisotropic heterogeneous media. Geophysics, 66: 294-307.

Crase, E., Pica, A., Noble, M., McDonald, J. and Tarantola, A., 1990. Robust elastic nonlinear waveform inversion: Application to real data. Geophysics, 55: 527-538.

De Basabe, J.D., Sen, M.K. and Wheeler, M.F., 2008. The interior penalty discontinuous Galerkin method for elastic wave propagation: grid dispersion. Geophys. J. Internat., 175: 83-93.

Duru, K., and Kreiss, G., 2012. A well-posed and discretely stable perfectly matched layer for elastic wave equations in second order formulation. Communic. Computat. Phys., 11: 1643.

Grote, M.J. and Sim, I., 2010. Efficient PML for the wave equation, arXiv preprint arXiv: 1001.0319.

Hastings, F.D., Schneider, J.B. and Broschat, S.L., 1996. Application of the perfectly matched layer (PML) absorbing boundary condition to elastic wave propagation. J. Acoust. Soc. Am., 100: 3061-3069.

Kim, Y., Min, D.J. and Shin, C., 2011. Frequency-domain reverse-time migration with source estimation. Geophysics, 76: S41-S49.

Komatitsch, D. and Martin, R., 2007. An unsplit convolutional perfectly matched layer improved at grazing incidence for the seismic wave equation. Geophysics, 72: SM155-SM167.

Komatitsch, D. and Vilotte, J.P., 1998. The spectral element method: an efficient tool to simulate the seismic response of 2D and 3D geological structures. Bull. Seismol. Soc. Am., 88: 368-392.

Komatitsch, D. and Tromp, J., 2003. A perfectly matched layer absorbing boundary condition for the second-order seismic wave equation. Geophys. J. Internat., 154: 146-153.

Kosloff, D., Queiroz Filho, A., Tessmer, E. and Behle, A., 1989. Numerical solution of the acoustic and elastic wave equations by a new rapid expansion method. Geophys. Prosp., 37: 383-394.

Ledbetter, H.M., 1977. Elastic properties of zinc: A compilation and a review. J. Phys. Chem. Ref. Data, 6: 1181-1203.

Li, Y. and Matar, O.B., 2010. Convolutional perfectly matched layer for elastic second-order wave equation. J. Acoust. Soc. Am., 127: 1318-1327.

Liu, Q.H. and Tao, J., 1997. The perfectly matched layer for acoustic waves in absorptive media. J. Acoust. Soc. Am., 102: 2072-2082.

Marfurt, K.J., 1984. Accuracy of finite-difference and finite-element modeling of the scalar and elastic wave equations. Geophysics, 49: 533-549.

Meza-Fajardo, K.C. and Papageorgiou, A.S., 2008. A nonconvolutional, split-field, perfectly matched layer for wave propagation in isotropic and anisotropic elastic media: Stability analysis. Bull. Seismol. Soc. Am., 98: 1811-1836.

Mora, P., 1987. Nonlinear two-dimensional elastic inversion of multioffset seismic data. Geophysics, 52: 1211-1228.

Pratt, R.G., Shin, C. and Hick, G.J., 1998. Gauss-Newton and full Newton methods in frequency-space seismic waveform inversion. Geophys. J. Internat., 133: 341-362.

Qi, Q. and Geers, T.L., 1998. Evaluation of the perfectly matched layer for computational acoustics. J. Computat. Phys., 139: 166-183.

Shin, C. and Cha, Y.H., 2008. Waveform inversion in the Laplace domain. Geophys. J. Internat., 173: 922-931.
Shin, C. and Cha, Y.H., 2009. Waveform inversion in the Laplace-Fourier domain. Geophys. J. Internat., 177: 1067-1079.
Sun, R. and McMechan, G.A., 2001. Scalar reverse-time depth migration of prestack elastic seismic data. Geophysics, 66: 1519-1527.
Tarantola, A., 1986. A strategy for nonlinear elastic inversion of seismic reflection data. Geophysics, 51: 1893-1903.
Thomsen, L., 1986. Weak elastic anisotropy. Geophysics, 51: 1954-1966.
Yan, J. and Sava, P., 2008. Isotropic angle-domain elastic reverse-time migration. Geophysics, 73: S229-S239.

APPENDIX

The final formulation of the PML for the 3D elastic wave equation with VTI media is

$$
\begin{aligned}
\rho(\partial^2 u/\partial t^2) = {} & (\partial/\partial x)[c_{11}(\partial u/\partial x) + \phi_{u,x} + c_{12}(\partial v/\partial y) + d_y(\partial \varphi_w/\partial z) \\
& + c_{13}(\partial w/\partial z) + d_z(\partial \varphi_v/\partial y)] \\
& + (\partial/\partial y)[c_{66}(\partial u/\partial y) + \phi_{u,y} + c_{66}(\partial v/\partial x) + d_z(\partial \varphi_v/\partial x) \\
& + (\partial/\partial z)[c_{44}(\partial u/\partial z) + \phi_{u,z} + c_{44}(\partial w/\partial x) + d_y(\partial \varphi_w/\partial x) \\
& - \rho(d_x + d_y + d_z)(\partial u/\partial t) \\
& - \rho(d_x d_y + d_y d_z + d_z d_x)u - \rho d_x d_y d_z \varphi_u \quad , \\
\\
\rho(\partial^2 v/\partial t^2) = {} & (\partial/\partial x)[c_{66}(\partial u/\partial y) + d_z(\partial \varphi_u/\partial y) + c_{66}(\partial v/\partial x) + \phi_{v,x}] \\
& + (\partial/\partial y)[c_{12}(\partial u/\partial x) + d_z(\partial \varphi_u/\partial x) + c_{11}(\partial v/\partial y) \\
& + \phi_{v,y} + c_{13}(\partial w/\partial z) + d_x(\partial \varphi_w/\partial z)] \\
& + (\partial/\partial z)[c_{44}(\partial v/\partial z) + \phi_{v,z} + c_{44}(\partial w/\partial x) + d_y(\partial \varphi_w/\partial x) \\
& - \rho(d_x + d_y + d_z)(\partial v/\partial t) \\
& - \rho(d_x d_y + d_y d_z + d_z d_x)v - \rho d_x d_y d_z \varphi_v \quad ,
\end{aligned}
\tag{A-1}
$$

$$\begin{aligned}\rho(\partial^2 w/\partial t^2) &= (\partial/\partial x)[c_{44}(\partial u/\partial z) + d_y(\partial \varphi_u/\partial z) + c_{44}(\partial w/\partial x) + \phi_{w,x}] \\ &+ (\partial/\partial y)[c_{44}(\partial v/\partial z) + d_x(\partial \varphi_v/\partial z) + c_{44}(\partial w/\partial y) + \phi_{w,y}] \\ &+ (\partial/\partial z)[c_{13}(\partial u/\partial x) + d_y(\partial \varphi_u/\partial x) + c_{13}(\partial v/\partial y) \\ &+ d_x(\partial \varphi_v/\partial y) + c_{33}(\partial w/\partial z) + \phi_{w,z}] \\ &- \rho(d_x + d_y + d_z)(\partial w/\partial t) \\ &- \rho(d_x d_y + d_y d_z + d_z d_x)w - \rho d_x d_y d_z \varphi_w \ ,\end{aligned}$$

and the ADEs are written as

$$\begin{aligned}&\partial \varphi_u/\partial t = u \ , \ \partial \varphi_v/\partial t = v \ , \ \partial \varphi_w/\partial t = w \ , \\ &\partial \phi_{u,x}/\partial t = -d_x \phi_{u,x} + c_{11}[(d_y + d_z - d_x)(\partial u/\partial x) + d_y d_z(\partial \varphi_u/\partial x)] \ , \\ &\partial \phi_{u,y}/\partial t = -d_y \phi_{u,y} + c_{66}[(d_z + d_x - d_y)(\partial u/\partial y) + d_z d_x(\partial \varphi_u/\partial y)] \ , \\ &\partial \phi_{u,z}/\partial t = -d_z \phi_{u,z} + c_{44}[(d_x + d_y - d_z)(\partial u/\partial z) + d_x d_y(\partial \varphi_u/\partial z)] \ , \\ &\partial \phi_{v,x}/\partial t = -d_x \phi_{v,x} + c_{66}[(d_y + d_z - d_x)(\partial v/\partial x) + d_y d_z(\partial \varphi_v/\partial x)] \ , \\ &\partial \phi_{v,y}/\partial t = -d_y \phi_{v,y} + c_{11}[(d_z + d_x - d_y)(\partial v/\partial y) + d_z d_x(\partial \varphi_v/\partial y)] \ , \\ &\partial \phi_{v,z}/\partial t = -d_z \phi_{v,z} + c_{44}[(d_x + d_y - d_z)(\partial v/\partial z) + d_x d_y(\partial \varphi_v/\partial z)] \ , \\ &\partial \phi_{w,x}/\partial t = -d_x \phi_{w,x} + c_{44}[(d_y + d_z - d_x)(\partial w/\partial x) + d_y d_z(\partial \varphi_w/\partial x)] \ , \\ &\partial \phi_{w,y}/\partial t = -d_y \phi_{w,y} + c_{44}[(d_z + d_x - d_y)(\partial w/\partial y) + d_z d_x(\partial \varphi_w/\partial y)] \ , \\ &\partial \phi_{w,z}/\partial t = -d_z \phi_{w,z} + c_{33}[(d_x + d_y - d_z)(\partial w/\partial z) + d_x d_y(\partial \varphi_w/\partial z)] \ .\end{aligned} \tag{A-2}$$